

Effects of metallic electrodes on the thermoelectric properties of zigzag graphene nanoribbons with periodic vacancies

David M T Kuo

*Department of Electrical Engineering and Department of Physics,
National Central University, Chungli, 320 Taiwan*

(Dated: May 8, 2023)

We theoretically analyze the thermoelectric properties of graphene quantum dot arrays (GQDAs) with line- or surface-contacted metal electrodes. Such GQDAs are realized as zigzag graphene nanoribbons (ZGNRs) with periodic vacancies. Gaps and minibands are formed in these GQDAs, which can have metallic and semiconducting phases. The electronic states of the first conduction (valence) miniband with nonlinear dispersion may have long coherent lengths along the zigzag edge direction. With line-contacted metal electrodes, the GQDAs have the characteristics of serially coupled quantum dots (SCQDs) if the armchair edge atoms of the ZGNRs are coupled to the electrodes. By contrast, the GQDAs have the characteristics of parallel QDs if the zigzag edge atoms are coupled to the electrodes. The maximum thermoelectric power factors of SCQDs with line-contacted electrodes of Cu, Au, Pt, Pd, or Ti at room temperature were similar or greater than $0.186nW/K$; their figures of merit were greater than three. GQDAs with line-contacted metal electrodes have much better thermoelectric performance than surface contacted metal electrodes.

I. INTRODUCTION

Charge transport through individual quantum dots with discrete levels exhibits an interesting phenomenon such as the Kondo effect and Coulomb blockade.[1] Quantum dots (QDs) have also been suggested as implementations of low-power devices. These low-power devices include single-electron transistors[2,3], single-photon sources[4-6], single-photon detectors[7] and single-electron heat engines[8]. Some applications of QD devices require both high efficiency and considerable output power. These applications require QD solids that can retain the size-tunable properties of QDs and possess the band transport characteristic of bulk semiconductors [9]. Although substantial effort has been devoted to producing such QD solids, experimental studies of the thermoelectric properties of such one-dimensional QD arrays are lacking [10,11]. Dot-size fluctuation is a challenge for thermoelectric devices made from 1D silicon QD arrays (QDAs) [12].

Recently, numerous studies have focused on two-dimensional (2D) materials such as graphenes [13], and 2D transition metal dichalcogenides (TMDs) and oxides [14–16]. Quasi-1D graphene nanoribbons (GNRs) can now be fabricated with atomic precision by using the bottom-up approach [17]; this approach can yield complex graphene-based nanostructures on-demand for quantum device applications [18–28]. The superlattices of zigzag GNRs (ZGNRs) behave as graphene QDAs (GQDAs) [29]. The phonon thermal conductance of GQDAs can be dramatically reduced by at least one order of magnitude compared with that of ZGNRs [30]. Therefore, GQDAs are expected to have promising applications in nanoscale energy harvesting.

Nevertheless, previous studies have demonstrated that the contact types of graphene and GNRs significantly influence electron transport between the electrodes [31–33]. To reduce the number of electron backward scat-

tering components, GNR devices can be produced using normal metal electrodes instead of graphene electrodes to improve the transmission coefficient [32]. In addition, the contact resistance of a graphene with line-contacted metal electrodes can be much smaller than that of a graphene with surface-contacted metal electrodes [33]. Other 2D materials also have this feature [34, 35]. These results all indicate that the interface properties arising from the presence of a contact junction is a key factor affecting the implementation of graphene-based or TMD-based electronic and thermoelectric devices.

Few studies have examined how the performance of GQDA thermoelectric devices is affected by the material properties and geometries of various contacting metals. In this study, we theoretically investigate the ballistic transport and thermoelectric properties of GQDAs coupled to various metal electrodes, as shown in Fig. 1; GQDAs are realized by ZGNRs with periodic vacancies. We have focused on the channel length between thermal contact shorter than the electron mean free path (λ_e) but longer than the phonon mean free path (λ_{ph}). We calculated the electrical conductance (G_e), Seebeck coefficient (S) and electron thermal conductance (κ_e) for different line-contacted metal electrodes and surface-contacted metal electrodes using the tight-binding model and Green's function. We find that the maximum thermoelectric power factor values of GQDAs with Cu, Au, Pt, Pd or Ti line-contacted electrodes can reach up to 79% of the power factor of the 1D theoretical limit at room temperature.

II. CALCULATION METHOD

A good approximation of the electronic states of a GQDA realized by ZGNRs with periodic vacancies is a tight-binding model with one p_z orbital per atomic site [29, 36]. The Hamiltonian of the GQDA, written,

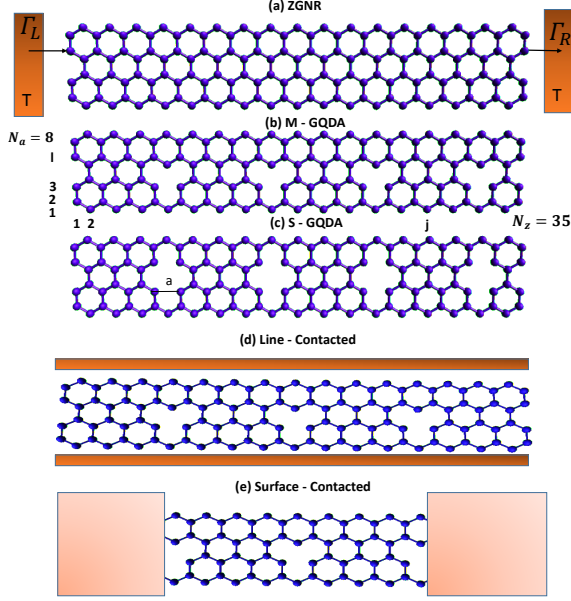


FIG. 1: Diagram of ZGNR without and with vacancies for $N_a = 8$ and $N_z = 35$. (a) Armchair edge atoms of ZGNRs coupled to metallic electrodes. Γ_L (Γ_R) denotes the tunneling rate of the electrons between the left (right) electrode and the leftmost (rightmost) carbon atoms of the armchair edges. T denotes the equilibrium temperature of the left (right) electrode. (b, c) Graphene quantum dot arrays (GQDAs) are realized by periodically removing one carbon and two carbons from the interior sites of ZGNRs. The distance between the nearest vacancies is $D = 4a$, where the lattice constant of graphene is $a = 2.46\text{\AA}$. (d) The zigzag edge atoms of GQDAs are coupled to the metal electrodes. (e) GQDAs with surface-contacted metal electrodes.

H_{GQDA} , is

$$H_{GQDA} = \sum_{\ell,j} E_{\ell,j} d_{\ell,j}^\dagger d_{\ell,j} \quad (1)$$

$$- \sum_{\ell,j} \sum_{\ell',j'} t_{(\ell,j),(\ell',j')} d_{\ell,j}^\dagger d_{\ell',j'} + h.c.,$$

where $E_{\ell,j}$ is the on-site energy for the p_z orbital in the ℓ th row and j th column. $d_{\ell,j}^\dagger$ ($d_{\ell,j}$) creates (destroys) one electron at the atom site labeled by (ℓ,j) where ℓ and j are the row and column indices, respectively, as depicted in Fig. 1. $t_{(\ell,j),(\ell',j')}$ describes the electron hopping energy from site (ℓ,j) to site (ℓ',j') . The tight-binding parameters used for GQDAs are $E_{\ell,j} = 0$ for the on-site energy and $t_{(\ell,j),(\ell',j')} = t_{pp\pi} = 2.7\text{ eV}$ for the nearest-neighbor hopping strength. Here, the electron-electron Coulomb interactions are neglected. Their effect is discussed in a subsequent section.

Thermoelectric coefficients, namely the electrical conductance (G_e), Seebeck coefficient (S) and electron thermal conductance (κ_e) were calculated using $G_e = e^2 \mathcal{L}_0$,

$S = -\mathcal{L}_1/(eT\mathcal{L}_0)$ and $\kappa_e = \frac{1}{T}(\mathcal{L}_2 - \mathcal{L}_1^2/\mathcal{L}_0)$ with \mathcal{L}_n ($n = 0, 1, 2$) defined as

$$\mathcal{L}_n = \frac{2}{h} \int d\varepsilon \mathcal{T}_{LR}(\varepsilon) (\varepsilon - \mu)^n \frac{\partial f(\varepsilon)}{\partial \mu}. \quad (2)$$

Here, $f(\varepsilon) = 1/(\exp^{(\varepsilon-\mu)/k_B T} + 1)$ is the Fermi distribution function of electrodes at equilibrium temperature T and chemical potential μ . $\mathcal{T}_{LR}(\varepsilon)$ denotes the transmission coefficient of a GQDA connected to electrodes, which can be calculated using the formula $\mathcal{T}_{LR}(\varepsilon) = 4\text{Tr}[\Gamma_L(\varepsilon)G^r(\varepsilon)\Gamma_R(\varepsilon)G^a(\varepsilon)]$ [37–39], where $\Gamma_L(\varepsilon)$ and $\Gamma_R(\varepsilon)$ denote the tunneling rate at the left and right leads, respectively, and $G^r(\varepsilon)$ and $G^a(\varepsilon)$ are the retarded and advanced Green's functions of the GQDA, respectively. The tunneling rates are described by the imaginary part of the self energy resulting from the coupling between the left (right) electrode with its adjacent GQDA atoms. Based on the tight-binding orbitals, $\Gamma_\alpha(\varepsilon)$ and Green's functions are matrices. For simplicity, Γ_α for interface carbon atoms has diagonal entries given by the same constant Γ_t . The magnitudes of Γ_t depend on the line- or surface-contacted metal electrodes [33]. The thermoelectric efficiency of graphene quantum dot arrays (GQDAs) is determined by the dimensionless figure of merit $ZT = S^2 G_e T / (\kappa_e + \kappa_{ph})$, where κ_{ph} denotes the phonon thermal conductance of GQDAs. First-principle calculations of κ_{ph} are beyond the scope of this article, so for simplicity, we calculate κ_{ph} using an empirical method described in ref. [39]. The phonon mean free path λ_{ph} has been measured to be reduced from 300–600 nm in a single-layer graphene to 10 nm in graphene nanostructures (see [40] and references therein). In this study, we chose zigzag graphene nanoribbons (ZGNRs) with $N_z = 127$ ($L_z = 15.5\text{ nm}$) because the channel length between thermal contacts satisfies the condition of being shorter than λ_e but longer than λ_{ph} .

III. RESULTS AND DISCUSSION

A. Electronic energy levels

Graphene with gapless characteristics has limited applications in devices [41, 42]. However, graphene with periodic vacancies has minibands, which enable its applications in thermoelectric devices at low temperatures [43,44]. To enable the graphene-based devices operating at room temperature, some studies have considered ZGNRs with periodic vacancies [45]. However, few studies have investigated how line- and surface-contacted metal electrodes affect the thermoelectric properties of ZGNRs with vacancies. The electron band structures of infinite ZGNRs without and with periodic vacancies are presented in Fig. 2. The band structures of infinite ZGNRs with various widths (N_a) have been extensively studied [41]. The localized zero-energy flat-band modes of the first subband are from $k = \frac{2\pi}{3a}$ to $\frac{\pi}{a}$ as $N_a \rightarrow \infty$.

In Fig. 2(a), the states of the first subband are the localized states for k within $k_c = 0.738\frac{\pi}{a} \leq k \leq \frac{\pi}{a}$, where k_c is determined by $k_c/2 = \arccos(N_a/(2N_a + 4))$ and $N_a = 8$ [36]. The edge state with the shortest decay length along the armchair direction occurs at $k = \frac{\pi}{a}$. When k deviates from $\frac{\pi}{a}$, the zigzag edges states form bonding and antibonding states, and the zero-energy modes disappear [Fig. 2(a)]. When $|E| \geq 2.16$ eV, we observe the second conduction and valence subbands. Because these are bulk states, this study focuses on the edge states of the first subband with $|E| \leq 2.16$ eV. For ZGNRs with periodic vacancies [Fig. 2(b) and Fig. 2(c)], the gapped energy regions are open and minibands are formed. ZGNR with periodic vacancies can be in the semiconducting phase as illustrated by the sizable central gap (0.959 eV) in Fig. 2(c). To reflect this phase difference, they are denoted metal GQDAs (M-GQDAs) and semiconductor GQDAs (S-GQDAs). Because the finite channel length is shorter than λ_e but longer than λ_{ph} , the length-dependent energy levels of GQDAs should be further clarified.

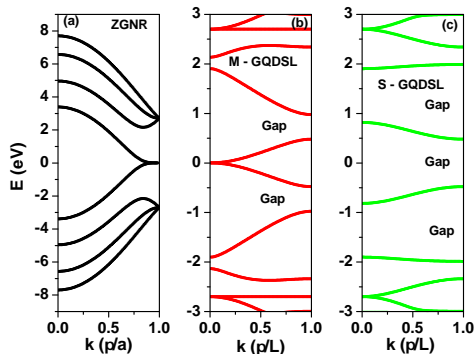


FIG. 2: Electronic band structures of infinite ZGNRs (a) without and (b, c) with periodic vacancies. The distance between the nearest vacancies is always $L = 4a$ in this article. The size of a super unit cell is characterized by $N_a = 8$ and $N_z = 8$.

To illustrate the characteristics of the energy levels in each miniband of Fig. 2(b) and 2(c), we present the calculated eigenvalues as functions of QD number N_{QD} (or $N_z = 8N_{QD} - 1$) in Fig. 3. The spectra reveal the transformation from the molecule-like state to band-like state as N_{QD} increases from 3 toward infinity (Fig. 2). In Fig. 3, the number of energy levels in each miniband is given by N_{QD} , demonstrating that finite-size ZGNRs with periodic vacancies exhibit the characteristics of GQDAs. A single GQD can be characterized by the size of $N_a = 8$ and $N_z = 7$, which results in four energy levels of $\varepsilon_{h,2} = -1.9024$ eV, $\varepsilon_{h,1} = -0.47905$ eV, $\varepsilon_{e,1} = 0.47905$ eV and $\varepsilon_{e,2} = 1.9024$ eV in the range of $|E| \leq 2.16$ eV. These four energy levels do not vary with N_{QD} . To understand this behavior, we calculate the eigenvalues of ZGNRs without periodic vacancies as a function of $N_z = 8N_{QD} - 1$ for $N_a = 8$ and obtain N_z -independent

$\varepsilon_{e(h),1}$ and $\varepsilon_{e(h),2}$. The wave functions of $\varepsilon_{e(h),1}$ and $\varepsilon_{e(h),2}$ of the ZGNRs are vanishingly small at $j = 8m$ (so-called nodes), where m is an integer. This explains the presence of N_{QD} -independent $\varepsilon_{e(h),1}$ and $\varepsilon_{e(h),2}$ in Fig. 3. The sinusoidal wave of $\varepsilon_{e(h),1}$ ($\varepsilon_{e(h),2}$) along the zigzag edges has a much longer coherence length than away from these edges. Although the periodic vacancies do not affect the energy levels of $\varepsilon_{e(h),1}$ and $\varepsilon_{e(h),2}$, they restrict and perturb some energy levels of ZGNRs. Therefore, they are called antidots [43–45].

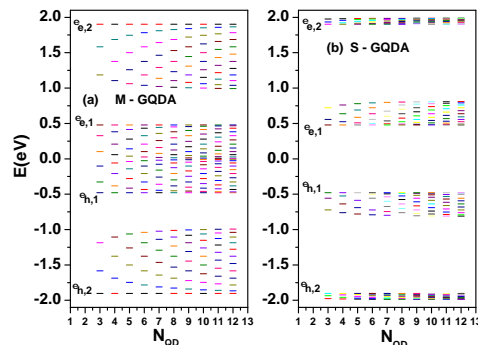


FIG. 3: Spectra of (a) M-GQDA and (b) S-GQDA as functions of N_{QD} . Each GQD in the GQDA structures has size $N_a = 8$ and $N_z = 7$. The length of the GQDA is $N_z = 8N_{QD} - 1$.

B. Line-contacted metal electrodes

When a graphene is coupled to metal electrodes, contact properties such as the Schottky barrier or ohmic contact and contact geometries can significantly affect the electron transport in graphene [33, 46–57]. Although many theoretical studies have attempted to clarify this key behavior from first principles, only qualitative results regarding Γ_t arising from the contact junction can be obtained due to theoretical limitations [58, 59]. In Fig. 4, we present that the calculated transmission coefficient of interface $T_c(\varepsilon)$ based on the configuration considered in [33], in which the authors introduced “super unit cells” with eight unit cells and investigated the armchair edge atoms of graphene coupled to various metal electrodes. Contact resistance $R_c = 1/G_{e,c}$ per unit cell is determined by $G_{e,c} = G_0 T_c(\varepsilon = 0)$, where $G_0 = 2e^2/h = 1/(12.9k\Omega) = 77.5\mu S$ is the quantum conductance and $T_c(\varepsilon = 0)$ is the contact transmission coefficient at the Fermi energy. In [33], the authors reported that $R_c = 13.3, 17.8, 18.6, 23.3$ and $31.7 k\Omega$ for Ti, Pd, Pt, Au and Cu, respectively. The Γ_t of each carbon atom at the interface can be obtained by fitting these contact resistances. We obtain the Γ_t values of Cu, Au, Pt, Pd, and Ti as $\Gamma_t = 0.495$ eV, $\Gamma_t = 0.603$ eV, $\Gamma_t = 0.693$ eV, $\Gamma_t = 0.72$ eV, and $\Gamma_t = 0.9$ eV, respectively.

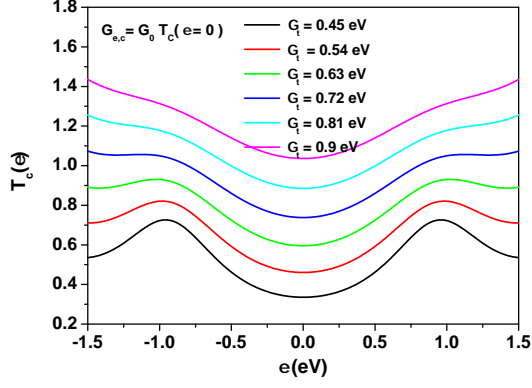


FIG. 4: Transmission coefficient at the metal–graphene interface per unit cell for various Γ_t values. Armchair edge atoms of graphene are coupled to metal electrodes. A super unit cell comprises 16 carbon atoms.

1. Armchair edge atoms coupled to electrodes

Based on the aforementioned Γ_t values, Fig. 5 presents the calculated $\mathcal{T}_{LR}(\varepsilon)$ of M-GQDA with $N_a = 8$ and $N_z = 127$ for various metal electrodes. The maximum $\mathcal{T}_{LR}(\varepsilon) = 1$ indicates that GQDAs behave as serially coupled QDs (SCQDs). Note that two energy levels $\varepsilon_{e(h)} = \pm 0.47905\text{eV}$ and $\varepsilon_{e(h)} = \pm 0.47179\text{eV}$ are too close to be resolved in the spectra of $\mathcal{T}_{LR}(\varepsilon)$. From Eq. (2), the area below the $\mathcal{T}_{LR}(\varepsilon)$ curve has a considerable effect on the thermoelectric coefficients. As illustrated in Fig. 5, the area below the $\mathcal{T}_{LR}(\varepsilon)$ curve increases with the tunneling rate. Moreover, these areas maintain a near-right triangle shape that exhibits a steep change with respect to ε on the sides of the $\varepsilon_{e,1}$ and $\varepsilon_{h,1}$ edges. For energy harvesting applications at room temperature, we must design a $\mathcal{T}_{LR}(\varepsilon)$ spectrum with a square form (SF) to obtain the optimal figure of merit and electrical power output.[60] However, no method has been developed for realizing a $\mathcal{T}_{LR}(\varepsilon)$ curve area with SF in a finite channel length ($L_z < \lambda_e$) between thermal contacts [39].

We then calculate the electrical conductance (G_e), Seebeck coefficient (S), power factor (PF), and figure of merit (ZT) of M-GQDAs at room temperature (Fig. 6). G_e , S , and PF are in units of $G_0 = 2e^2/h$, $k_B/e = 86.25\mu\text{V}/\text{K}$, and $2k_B^2/h = 0.575\text{pW}/\text{K}^2$, respectively. Unlike G_e , S is less sensitive to variations in Γ_t [Fig.6(b)]. The behavior of S can be approximated by $S = -\frac{\pi^2 k_B^2 T}{3e} \frac{\partial \ln(G_e(\mu, T))}{\partial \mu}$. The maximum PF and ZT values are given by μ in the gap region. The trend of ZT with respect to various metal electrodes is determined by the power factor ($PF = S^2 G_e$) because the thermal conductance of GQDAs is dominated by phonon thermal conductance κ_{ph} . We calculated the dimensionless $ZT = S^2 G_e T / (\kappa_e + \kappa_{ph})$ with $\kappa_{ph} = F_s \kappa_{ph, ZGNR}$, where $\kappa_{ph, ZGNR} = \frac{\pi^2 k_B^2 T}{3h}$ is the phonon thermal conductance

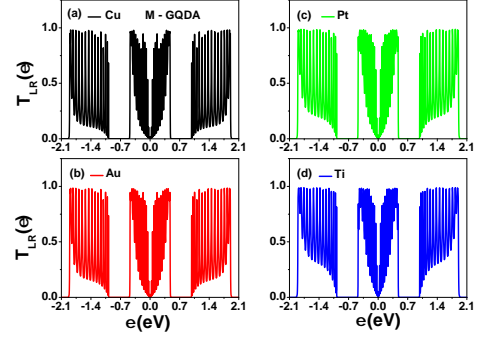


FIG. 5: Transmission coefficient $\mathcal{T}_{LR}(\varepsilon)$ of a finite M-GQDA as functions of ε for various line-contacted metal electrodes at $N_a = 8$ ($L_a = 0.71\text{nm}$) and $N_z = 127$ ($L_z = 15.5\text{nm}$). Diagrams (a), (b), (c), and (d) correspond to Cu, Au, Pt, and Ti, respectively.

of an ideal ZGNR [61] and $F_s = 0.1$ denotes a reduction factor resulting from periodic vacancies in ZGNRs [30, 44]. The results in Fig. 6 imply that $ZT > 3$ can be realized if GQDAs are considered to be coupled to metallic electrodes. The four investigated metal electrodes have similar maximum PF and ZT values; the maximum PF can reach 79% of the theoretical limit for 1D systems of $PF_{QB} = 1.2659(\frac{2k_B^2}{h})$ [60]. ZGNRs are graphene-based 1D topological insulators (TIs), and ZT of 1D TIs greater than 3 has been theoretically demonstrated in the absence of periodic vacancies [62]. The ZT values of 1D TIs tend to be at their maximum when μ is near the minimum value of the second subband, as shown in Fig. 2(a) ($|E| = 2.16\text{eV}$).

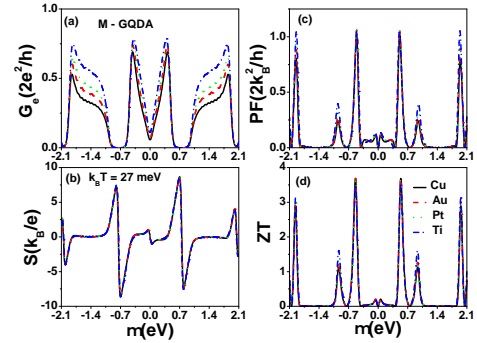


FIG. 6: (a) Electrical conductance G_e , (b) Seebeck coefficient S , (c) power factor ($PF = S^2 G_e$), and (d) figure of merit ZT as functions of μ for various metal electrodes at $k_B T = 27\text{meV}$.

In Fig. 6(b), the gaps between the minibands substantially enhance the maximum S values, suggesting that the thermoelectric properties of S-GQDAs with a large central band gap should be investigated. The calculated

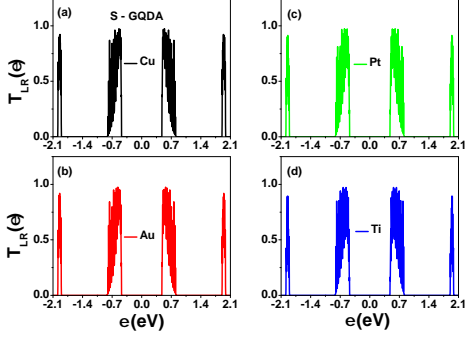


FIG. 7: Transmission coefficient $\mathcal{T}_{LR}(\varepsilon)$ of a finite S-GQDA as functions of ε for different line-contacted metal electrodes at $N_a = 8$ ($L_a = 0.71\text{nm}$) and $N_z = 127$ ($L_z = 15.5\text{nm}$). Diagrams (a), (b), (c), and (d) correspond to Cu, Au, Pt, and Ti, respectively.

transmission coefficients of S-GQDAs with various line-contacted metal electrodes are presented in Fig. 7. The miniband widths of S-GQDAs are much smaller than those of M-GQDAs, resulting in a greatly reduced area of their $\mathcal{T}_{LR}(\varepsilon)$ curves. Fig. 8 presents the calculated G_e , S , power factor PF , and ZT as functions of μ at room temperature. Due to electron-hole symmetry, we considered the range of chemical potential $\mu \geq 0$. The G_e spectra of the first miniband remains triangular as in Fig. 6(a), but the steep change with respect to μ is toward the central gap. Because of large gaps, the maximum Seebeck coefficients in Fig. 8(b) are almost twice as large as those in Fig. 6(b). The maximum power factor $PF_{max}(\mu = 0.45\text{eV}) = 0.9682$ and figure of merit $ZT_{max}(\mu = 0.427\text{eV}) = 3.442$ occur at the chemical potentials near $\varepsilon_{e,1} = 0.47905\text{eV}$ for Cu electrodes. The κ_{ph} value used in the analysis is the same as that in Fig. 6(d). A comparison of the maximum ZT in Fig. 8(d) and 6(d) reveals that it did not increase despite large increase in the maximum value of S . For $\kappa_{ph} \gg \kappa_e$, the increase of G_e also has a substantial effect. If the miniband width was small, G_e was suppressed in the gap region. In Fig. 8(c) and 8(d), $PF_{max,2}$ and $ZT_{max,2}$ are also smaller than $PF_{max,1}$ and $ZT_{max,1}$, respectively. These results indicate that increasing electrical power output requires not only large gaps but also relatively wide miniband widths.

2. Zigzag edge atoms coupled to electrodes

Our previous study demonstrated that the electron transport of finite ZGNRs is significantly affected by the armchair or zigzag edge sides coupled to electrodes [38]. According to [59], most edge-oxidized modifications dramatically change the electron band structures of ZGNRs. Therefore, we do not consider edge-oxidized GNRs in the following discussion. The contact resistance of Cr/X/graphene was calculated in [49], in which the zigzag

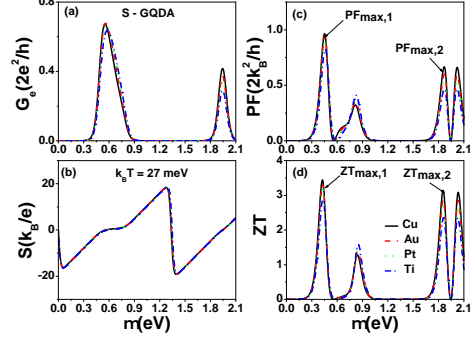


FIG. 8: (a) Electrical conductance G_e , (b) Seebeck coefficient S , (c) power factor $PF = S^2 G_e$, and (d) figure of merit (ZT) of S-GQDSLs as functions of μ for various metal electrodes at $k_B T = 27\text{meV}$.

edge atoms of graphene were coupled to Cr by various atomic bridges (H, F, O, or S). Due to the large binding distance, a high contact resistance was observed in the Cr/H/graphene structure. We adopted $\Gamma_t = 9\text{meV}$ and $\Gamma_t = 45\text{meV}$ for Cr/H/GQDAs and Cr/F/GQDAs, respectively, to calculate G_e as functions of μ at zero temperature (Fig. 9) for M-GQDAs and S-GQDAs with $N_a = 8$ and $N_z = 127$. In Fig. 9, the spectra of G_e are larger than quantum conductance $G_0 = \frac{2e^2}{h}$, demonstrating that GQDAs behave as parallel QDs when the zigzag edge atoms of M-GQDAs and S-GQDAs are coupled to the metal electrodes. In the parallel QD configuration, the spectra resulting from electronic states near the zero-energy modes of M-GQDAs and the high-energy modes of the first minibands of S-GQDAs substantially differ from the spectra in Fig. 5 and Fig. 7.

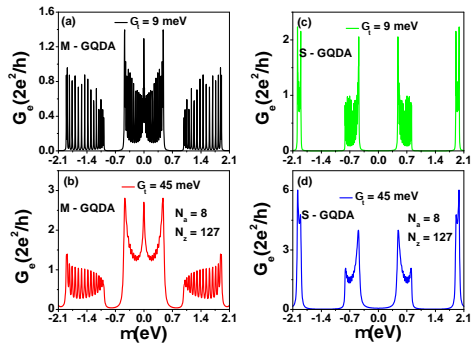


FIG. 9: Electrical conductance as functions of μ for $\Gamma_t = 9\text{meV}$ and $\Gamma_t = 45\text{meV}$ for (a,b) M-GQDAs and (c,d) S-GQDAs. Their sizes are $N_a = 8$ ($L_a = 0.71\text{nm}$) and $N_z = 127$ ($L_z = 15.5\text{nm}$).

Fig. 10 presents the calculated S and PF of M-GQDAs and S-GQDAs at room temperature ($k_B T = 27\text{meV}$). The maximum S is severely degraded for a parallel QD

configuration with a short channel length of $L_a = 0.71$ nm compared with the maximum S values of Fig. 6 and Fig. 8. This is attributable to the highly enhanced G_e in the gap region, which is similar to the metal-induced gap states in metal-semiconductor Schottky junctions [63]. When the zigzag edge atoms are coupled to the metal electrodes, the miniband edge states are readily extended into the gap regions if the channel length is short. Although the maximum PF in Fig. 10 is much larger than $PF_{QB} = 1.2659(\frac{2k_B^2}{h})$, their ZT values are less than one due to remarkable increases in electron thermal conductance (κ_e) and phonon thermal conductance (κ_{ph}).

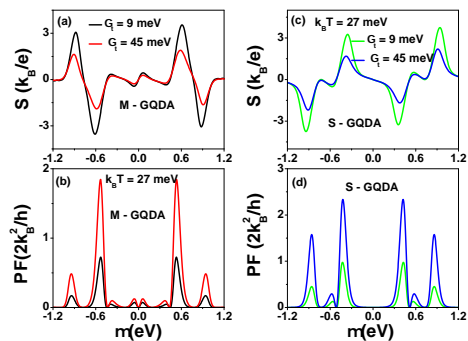


FIG. 10: (a) Seebeck coefficient and (b) power factor of M-GQDAs and (c,d) S-GQDAs as functions of μ for two tunneling rates at $k_B T = 27$ meV. Other physical parameters are the same as those in Fig. 9.

C. Surface-contacted metal electrodes

Few experimental studies have reported the transport and thermoelectric properties of GNRs due to the difficulty of applying the line-contacted technique [64]. However, surface-contacted metal electrodes are straightforward to lay out in an experiment. Therefore, experimental methods are preferable for revealing the thermoelectric properties of GNRs with surface-contacted electrodes. Many theoretical studies have demonstrated that the surface contact resistance is one to three orders of magnitude greater than the line contact resistance [33, 46–57], indicating that Γ_t may be extremely small. The calculated transmission coefficient of M-GQDA as functions of μ for various Γ_t values is presented in Fig. 11; the two outer GQDs are coupled to metal electrodes. The structure has 28 carbon atoms, including 6 carbon atoms each located at zigzag edge sites under the surface-contacted left (right) metal electrode. Due to the small Γ_t values, the peaks of the $\mathcal{T}_{LR}(\varepsilon)$ spectra are very narrow. These molecule-like spectra indicate degraded electrical conductance at room temperature.

Fig. 12 presents the calculated G_e , κ_e , PF , and ZT as functions of μ at different temperatures with surface-

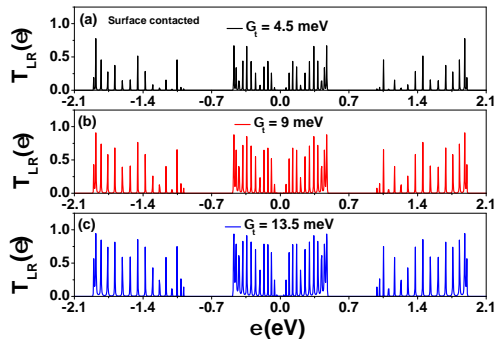


FIG. 11: Transmission coefficient of an M-GQDA with surface-contacted metal electrodes and $N_a = 8$ and $N_z = 127$ as functions of ε for various Γ_t values. (a), (b), and (c) correspond to $\Gamma_t = 4.5, 9,$ and 13.5 meV, respectively.

contacted metal electrodes. The maximum electrical conductance $G_e = 0.25G_0$ at room temperature is much smaller than that in Fig.6(a). Unlike the behavior of G_e with respect to temperature, electron thermal conductance κ_e is enhanced as the temperature increases. Here, κ_e is in units of $\kappa_0 = 0.62nW/K$. The increase in the maximum PF with decreasing temperature is attributable to the enhancement of S , which is a highly nonlinear function of temperature. In the calculation of ZT , κ_{ph} is the same as that in Fig. 5. At room temperature, the maximum value of $ZT(\mu = 0.535eV) = 1.9927$ is less than three. However, the maximum PF and ZT values increase with decreasing temperature. If the spectra of G_e have molecule-like characteristics, the thermoelectric performance of GQDAs remains acceptable in the low-temperature region [65].

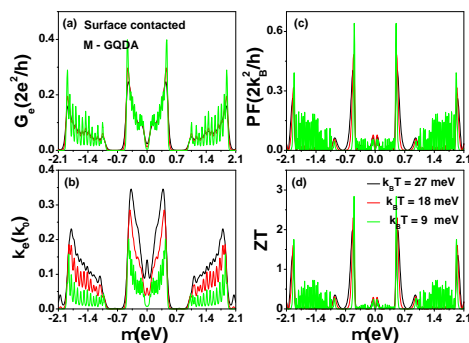


FIG. 12: (a) Electrical conductance, (b) electron thermal conductance, (c) power factor, and (d) figure of merit as functions of μ for various temperatures for M-GQDA with surface-contacted metal electrodes. $\Gamma_t = 14.5$ meV. Other physical parameters are the same as in Fig. 11.

The molecule-like or band-like spectra of GQDAs are determined by not only the lengths of the GQDAs but

also the contact geometry. In the line-contacted metal electrodes, the spectra of finite GQDAs have band-like characteristics due to the large Γ_t values. By contrast, the spectra of finite GQDAs with surface-contacted metal electrodes have molecule-like characteristics. We did not investigate the effect of electron–electron Coulomb interactions in this study. Although electron Coulomb interactions are strong in small GQDAs ($L_a = 0.71$ nm and $L_z = 15.5$ nm), their effects on the thermoelectric quantities can be neglected if electron transport is dominated by the thermionic-assisted tunneling procedure (TATP), which occurs at a distance of μ away from the minibands. The thermionic electron population in the minibands is very dilute if μ is located inside the gap. Hence, electron correlation functions arising from electron Coulomb interactions are small [65–67]. The calculated maximum PF and ZT are therefore valid in the TATP.

E-mail address: mtkuo@ee.ncu.edu.tw

IV. CONCLUSION

Although ZGNRs have metallic phases, the minibands and gaps are formed in ZGNRs with periodic vacancies, which behave as GQDAs. Such GQDAs can host metallic and semiconductor phases. The edge states of the first conductance and valence minibands, such as $\varepsilon_{e(h),1}$, are localized edge states along the armchair edge direction, whereas they have very long coherent lengths along the zigzag edge direction. The designed GQDAs have sufficiently large gaps and miniband widths to be applied in thermoelectric devices operating at room temperature. With line-contacted metal electrodes, the maximum power factor (figure of merit) of the M-GQDAs at room temperature is larger than that of the S-GQDAs due to the wider miniband widths of the M-GQDAs. The GQDAs behave as serially coupled QDs (SCQDs) if the armchair edge atoms are coupled to the metal electrodes. By contrast, the GQDAs behave as parallel-coupled QDs if zigzag edge atoms are coupled to metal electrodes. For SCQDs with line-contacted electrodes, the maximum power factor values of GQDAs with different metal electrodes (Cu, Au, Pt, Pd, or Ti) at room temperature can reach 79% of the theoretical limit of 1D systems, and their figures of merit are greater than three. If surface-contacted metal electrodes are used, the spectra of electrical conductance of the finite M-GQDAs have molecule-like characteristics because of high contact-surface resistance. The thermoelectric power factor and figures of merit of the M-GQDAs at room temperature are smaller than those of the line-contacted M-GQDAs; however, their ZT values can reach three at low temperatures.

Acknowledgments

We thank Yia-Chung Chang for their valuable intellectual input.

This work was supported by the Ministry of Science and Technology (MOST), Taiwan under Contract No. 110-2119-M-008-006-MBK.

- ¹ Haug H, and Jauho A P, Quantum Kinetics in Transport and Optics of Semiconductors (Springer, Heidelberg, 1996)
- ² Guo L J, Leobandung E and Chou S Y, A silicon single-electron transistor memory operating at room temperature, 1997 Science **275** 649
- ³ Postma H W C, Teepen T, Yao Z, Grifoni M and Dekker C, Carbon nanotube single-electron transistors at room temperature, 2001 Science **293** 76
- ⁴ Michler P, Imamoglu A, Mason M D, Carson P J, Strouse G F and Buratto S K, Quantum correlation among photons from a single quantum dot at room temperature, 2000 Nature **406** 968
- ⁵ Santori C, Fattal D, Vuckovic J, Solomon G S and Yamamoto Y, Indistinguishable photons from a single-photon device, 2002 Nature **419** 549
- ⁶ Chang W H, Chen W Y, Chang H S, Hsieh T P, and Hsu T M, Efficient single-photon sources based on low-density quantum dots in photonic-crystal nanocavities, 2006 Phys. Rev. Lett. **96** 117401
- ⁷ Gustavsson S, Studer M, Leturcq R, Ihn T, Ensslin K, Driscoll D C and Gossard A C, Frequency-selective single-photon detection using a double quantum dot, 2007 Phys. Rev. Lett. **99** 206804
- ⁸ Josefsson M, Svilans A, Burke A M, Hoffmann E A, Fahlvik S, Thelander C, Leijnse M and Linke H, A quantum-dot heat engine operating close to the thermodynamic efficiency limits, 2018 Nature Nanotechnology **13** 920
- ⁹ Kagan C R and Murry C B, Charge transport in strongly coupled quantum dot solids, 2015 Nature Nanotechnology **10** 1013
- ¹⁰ Harman T C, Taylor P J, Walsh M P and LaForge B E, Quantum dot superlattice thermoelectric materials and devices, 2002 Science **297** 2229
- ¹¹ Talgorn E, Gao Y, Aerts M, Kunneman L T, Schins J M, Savenije T J, Marijn A. van Huis, Herre S. J. van der Zant, Houtepen Arjan J and Siebbeles Laurens D A, Unity quantum yield of photogenerated charges and band-like transport in quantum-dot solids, 2011 Nature Nanotechnology **6** 733
- ¹² Lawrie W I L, Eenink H G J, Hendrickx N W, Boter J M, Petit L, Amitonov S V, Lodari M, Wuetz Paquelet B, Volk C. and Philips S G J et al, Quantum dot arrays in silicon and germanium, 2020 Appl. Phys. Lett. **116** 080501
- ¹³ Novoselov K S, Geim A K, Morozov S V, Jiang D, Zhang Y, Dubonos S V, Grigorieva I V and Firsov A A, Electric field effect in atomically thin carbon films, 2004 Science **306** 666
- ¹⁴ Geim A K and Grigorieva I V, Van der Waals heterostructures, 2013 Nature **499** 419
- ¹⁵ Novoselov K S, Mishchenko A, Carvalho A and Neto A H C, 2D materials and van der Waals heterostructures, 2016 Science **353** aac9439
- ¹⁶ Desai S B, Seol G, Kang J S, Fang H, Battaglia C, Kapadia R, Ager J W, Guo J and Javey A, Strain-Induced Indirect to Direct Bandgap Transition in Multi layer WSe₂, 2014 Nano Lett. **14** 4592
- ¹⁷ Cai J, Ruffieux P, Jaafar R, Bieri M, Braun T, Blankenburg S, Muoth M, Seitsonen A P, Saleh M, Feng X, Mullen K and Fasel Roman, Atomically precise bottom-up fabrication of graphene nanoribbons, 2010 Nature **466** 470
- ¹⁸ Liu J Z, Li B W, Tan Y Z, Giannakopoulos A, Sanchez-Sanchez C, Beljonne D, Ruffieux P, Fasel R, Feng X L and Mullen K, Toward Cove-Edged Low Band Gap Graphene Nanoribbons, 2015 J. Am. Chem. Soc. **137** 6097
- ¹⁹ Chen Y C, Cao T, Chen C, Pedramraz Z, Haberer D, Oteyza D G de, F. Fischer R, Louie S G and Crommie M F, Molecular bandgap engineering of bottom-up synthesized graphene nanoribbon heterojunctions, 2015 Nature Nanotechnology **10** 156
- ²⁰ Ruffieux P, Wang S, Yang B, Sacher-Sacher C, Liu J, Di-enel T, Talirz L, Shinde P, Pignedoli C A, Passerone D, Dumlaff T, Feng X, Mullen K and Fasel R, On-surface synthesis of graphene nanoribbons with zigzag edge topology, 2016 Nature **531** 489
- ²¹ Groning O, Wang S, Yao X, Pignedoli C A, Barin G B, Daniels C, Cupo A, Meunier V, Feng X, Narita A, Muellen K, Ruffieux P and Fasel R, Engineering of robust topological quantum phases in graphene nanoribbons, 2018 Nature **560** 209
- ²² Rizzo D J, Veber G, Cao T, Bronner C, Chen T, Zhao F, Rodriguez H, Louie S G, Crommie M F and Fischer F R, Topological band engineering of graphene nanoribbons, 2018 Nature **560** 204
- ²³ Yan L H and Liljeroth P, Engineered electronic states in atomically precise artificial lattices and graphene nanoribbons, 2019 ADVANCES IN PHYSICS: X **4** 1651672
- ²⁴ Rizzo D J, Veber G, Jiang J W, McCurdy R, Bronner T, Cao T, Chen T, Louie Steven G, Fischer F R and Crommie M F, Inducing metallicity in graphene nanoribbons via zero-mode superlattices, 2020 Science **369** 1597
- ²⁵ Sun Q, Yan Y, Yao X L, Mullen K, Narita A, Fasel R and Ruffieux P, Evolution of the Topological Energy Band in Graphene Nanoribbons , 2021 J. Phys. Chem. Lett. **12** 8679
- ²⁶ Rizzo D J, Jiang J W, Joshi D, Veber G, Bronner C, Durr R A, Jacobse P H, Cao T, Kalayjian A, Rodriguez H, Butler P, Chen T, Louie Steven G, Fischer F R and Crommie M F, Rationally Designed Topological Quantum Dots in Bottom-Up Graphene Nanoribbons, 2021 ACS Nano **15** 20633
- ²⁷ Wang X, Ma J, Zheng W H, Osella S, Arisnabarreta N, Droste J, Serra J, Ivashenko O, Lucotti A, Beljonne D, Bonn M, Liu X Y, Hansen M R, Tommasini M, Feyter S De, Liu J Z, Wang H I and Feng X L, Cove-Edged Graphene Nanoribbons with Incorporation of Periodic Zigzag-Edge Segments, 2022 J. Am. Chem. Soc. **144** 228
- ²⁸ Almeida P A and Martins G B, Thermoelectric transport properties of armchair graphene nanoribbon heterostructures, 2022 J. Phys: Condens. Matter **34** 335302
- ²⁹ Topsakal M, Sevincli H and Ciraci S, Spin confinement in the superlattices of graphene ribbons, 2008 Appl. Phys. Lett. **92** 173118
- ³⁰ Sevincli H and Cuniberti G, Enhanced thermoelectric figure of merit in edge-disordered zigzag graphene nanoribbons, 2010 Phys. Rev. B **81** 113401
- ³¹ Darancet P, Olevano V and Mayou D, Coherent Electronic Transport through Graphene Constrictions: Sub-wavelength Regime and Optical Analogy, 2009 Phys. Rev. Lett. **102** 136803
- ³² Liang G C, Neophytou N, Lundstrom M S and Nikonov D E, Contact effects in graphene nanoribbon transistors, 2008 Nano. Lett. **8** 1819

- ³³ Matsuda Y, Deng W Q and Goddard III W A, Contact Resistance for "End-Contacted" Metal-Graphene and Metal-Nanotube Interfaces from Quantum Mechanics, 2010 J. Phys. Chem. C. **114** 17845
- ³⁴ Shen P C, Su C, Lin Y X, Chou A S, Cheng C C, Park J H, Chiu M H, Lu A Y, Tang H L, Tavakoli M M, Pitner G, Ji X, Cai Z Y, Mao N N, Wang J T, Tung J V, Li C, Bokor J, Zettl A, Wu C I, Palacios T, Li L J and Kong J, Ultralow contact resistance between semimetal and monolayer semiconductors, 2021 Nature **593** 212
- ³⁵ Chen R S, Ding G L, Zhou Y and Han S T, Fermi-level depinning of 2D transition metal dichalcogenide transistors, 2021 J. Mater. Chem. C, **9** 11407
- ³⁶ Wakabayashi K, Sasaki K, Nakanishi T and Enoki T, Electronic states of graphene nanoribbons and analytical solutions, 2010 Sci. Technol. Adv. Mater. **11** 054504
- ³⁷ Kuo D M T, Thermoelectric and electron heat rectification properties of quantum dot superlattice nanowire arrays, 2020 AIP Advances **10** 045222
- ³⁸ Kuo D M T, Effects of zigzag edge states on the thermoelectric properties of finite graphene nanoribbons, 2022 Jpn. J. Appl. Phys. **61** 075001
- ³⁹ Kuo D M T and Chang Y C, Contact Effects on Thermoelectric Properties of Textured Graphene Nanoribbons, 2022 Nanomaterials **12** 3357
- ⁴⁰ Xu Y, Li Z Y, and Duan W H, Thermal and thermoelectric properties of graphene, 2014 Small **10** 2182
- ⁴¹ Nakada K, Fujita M, Dresselhaus G and Dresselhaus M S, Edge state in graphene ribbons: Nanometer size effect and edge shape dependence, 1996 Phys. Rev. B **54** 17954
- ⁴² Wakabayashi K, Fujita M, Ajiki H and Sgrist M, Electronic and magnetic properties of nanographite ribbons, 1999 Phys. Rev. B **59** 8271
- ⁴³ Gunst T, Markussen T, Jauho A P, and Brandbyge M, Thermoelectric properties of finite graphene antidot lattices, 2011 Phys. Rev. B **84** 155449
- ⁴⁴ Chang P H, Bahramy M S, Nagaosa N and Nikolic B K, Giant Thermoelectric Effect in Graphene-Based Topological Insulators with Heavy Adatoms and Nanopores, 2014 Nano Lett. **14** 3779
- ⁴⁵ Zhang Y T, Li Q M, Li Y C, Zhang Y Y and Zhai F, Band structures and transport properties of zigzag graphene nanoribbons with antidot array, 2010 J. Phys: Condens. Matter **22** 315304
- ⁴⁶ Chu T and Chen Z, Understanding the Electrical Impact of Edge Contacts in Few-Layer Graphene, 2014 ACS Nano **8** 3584
- ⁴⁷ Gong C, McDonnell S, Qin X Y, Azcatl A, Dong H, Chabal Y J, Cho K, and Wallace R M, Realistic Metal-Graphene contact structures, 2014 ACS Nano **8** 642
- ⁴⁸ Song S M, Kim T Y, Sul O J, Shin W C and Cho B J, Improvement of graphene-metal contact resistance by introducing edge contacts at graphene under metal, 2014 Appl. Phys. Lett. **104** 183506
- ⁴⁹ Gao Q and Guo J, Role of chemical termination in edge contact to graphene, 2014 APL Mater. **2** 056105
- ⁵⁰ Matsuda Y, Deng W Q, and Goddard III W A, Contact resistance properties between nanotubes and various metals from quantum mechanics, 2007 J. Phys. Chem. C **111** 11113
- ⁵¹ Massen J, Ji W, and Guo H, First principles study of electronic transport through a Cu(111)/graphene junction. 2010 Appl. Phys. Lett. **97** 142105
- ⁵² Barraza-Lopez S, Vanevic M, Kindermann M and Chou M Y, Effects of Metallic Contacts on Electron Transport through Graphene, 2010 Phys. Rev. Lett. **104** 076807
- ⁵³ Shen C, Liu J, Jiao N, Zhang C X, Xiao H, Wang R Z and Sun L Z, Transport properties of graphene/metal planar junction, 2014 Phys. Lett. A **378** 1321
- ⁵⁴ Ran Q, Gao M, Guan X, Wang Y and Yu Z, First principles investigation on bonding formation and electronic structure of metal graphene contacts, 2009 Appl. Phys. Lett. **94** 103511
- ⁵⁵ Stokbro K, Engelund M and Blom A, Atomic-scale model for the contact resistance of the nickel-graphene interface, 2012 Phys. Rev. B **85** 165442
- ⁵⁶ Ma B, Cheng G, Wen Y W, Chen R, Cho K G and Shan B, Modulation of contact resistance between metal and graphene by controlling the graphene edge, contact area, and points defects: An ab initio study, 2014 J. Appl. Phys. **115** 183708
- ⁵⁷ Qin H C, Lu W C and Bernholca J, Ab initio simulations of metal contacts for graphene-based devices, 2022 J. Appl. Phys. **131** 214301
- ⁵⁸ Yang L, Park C H, Son Y W, Cohen Marvin L, and Louie Steven G, Quasiparticle Energies and Band Gaps in Graphene Nanoribbons, 2007 Phys. Rev. Lett. **99** 186801
- ⁵⁹ Lee G and Cho K, Electronic structures of zigzag graphene nanoribbons with edge hydrogenation and oxidation, 2009 Phys. Rev. B **79** 165440
- ⁶⁰ R. S. Whitney, Most Efficient Quantum Thermoelectric at Finite Power Output, 2014 Phys. Rev. Lett. **112** 130601
- ⁶¹ Zheng H, Liu H J, Tan X J, Lv H Y, Pan L, Shi J and Tang X F, Enhanced thermoelectric performance of graphene nanoribbons, 2012 Appl. Phys. Lett. **100** 093104
- ⁶² Xu Y, Gan Z and Zhang S C, Enhanced Thermoelectric Performance and Anomalous Seebeck Effects in Topological Insulators, 2014 Phys. Rev. Lett. **112** 226801
- ⁶³ Golizadeh-Mojarad R and Datta S, Effect of contact induced states on minimum conductivity in graphene, 2009 Phys. Rev. B **79** 085410
- ⁶⁴ Cusati T, Fiori G, Gahoi A, Passi V, Lemme M C, Fortunelli A, and Iannaccone G, Electrical properties of graphene-metal contacts, 2017 Scientific Reports **7** 5109
- ⁶⁵ Kuo D M T and Chang Y C, Thermoelectric and thermal rectification properties of quantum dot junctions, 2010 Phys. Rev. B **81** 205321
- ⁶⁶ Kuo D M T, Shiau S Y and Chang Y C, Theory of spin blockade, charge ratchet effect, and thermoelectrical behavior in serially coupled quantum dot system, 2011 Phys. Rev. B **84** 245303
- ⁶⁷ Kuo D M T, Chen C C and Chang Y C, Large enhancement in thermoelectric efficiency of quantum dot junctions due to increase of level degeneracy, 2017 Phys. Rev. B **95** 075432